Ninth International Conference on
THIN-WALLED STRUCTURES – ICTWS2023
Sydney, Australia, Nov 29 – Dec 1, 2023

EXAMINING THE VIABILITY AND APPLICABILITY OF COLD METAL TRANSFER WELDING TECHNOLOGY FOR COLD-FORMED STEEL STRUCTURAL MEMBERS

Bishal Naik* and Mahendrakumar Madhavan**

* Research Scholar, Department of Civil Engineering, IIT Hyderabad, India
e-mail: ce20resch11001@iith.ac.in

** Professor, Department of Civil Engineering, IIT Hyderabad, India
e-mail: mkm@ce.iith.ac.in

Keywords: Cold-Formed Steel built-up sections, CMT welding, Flare v-groove welds, AISI design standard

Abstract. *Cold-Formed Steel (CFS) structural members have inherent challenges for conventional welding techniques such as Metal Inert Gas (MIG) or Tungsten Inert Gas (TIG) welding. In contrast, a novel and innovative welding technique, Cold Metal Transfer (CMT), has been proposed for CFS welded sections. In this study, a set of systematic welding trials were conducted to calibrate the welding parameters for CFS sections welded back-to-back via flare v-groove welds, using copper-coated steel wire ER70S-6 as a filler material and moderate-strength CFS sheets of grade 300 as the parent material. The welding trials involved different combinations of welding current, trolley speed of the welding torch, and thickness of the CFS sheets. The weld bead geometry was examined qualitatively and quantitatively using metallographic techniques, including the analysis of macroscopic images to determine the throat depth of CMT flare v-groove welds. The results demonstrated that the CMT welding technique is a feasible option for automated welding of CFS welded sections. Additionally, a set of calibrated welding parameters to achieve a specific thickness of weld is proposed. This study also focused on understanding the behaviour of flare v-groove welds on back-to-back connected CFS sections subjected to longitudinal shear. Lap shear tests were carried out on unlipped channels and hat sections of different cross-section dimensions, weld thickness, and weld length. The lap shear specimens primarily failed either in traverse plate tearing of parent material or brittle fracture of weld at the weld contours. The appropriateness of American Iron and Steel Institute (AISI) shear design strength equations for flare v-groove welds was verified, and preliminary design guidelines are provided addressing the lacunae in AISI design standard. Additionally, a limiting ratio is proposed which can accurately predict the failure mode of longitudinal CMT flare v-groove welds subjected to longitudinal shear. Overall, the study demonstrates that CMT welding is a feasible option for automated welding of CFS welded sections.*

1 INTRODUCTION

Cold Formed Steel (CFS) has gained widespread usage in the construction industry due to its numerous advantages over conventional hot-rolled steel. One notable advantage is its flexibility in cross-section shape, leading to increased material usage efficiency. However, the typical slender, thin-walled, singly-symmetric cross-sections of CFS make them structurally susceptible to instability failures, which restricts their effective use as primary structural components in residential constructions. CFS built-up sections offer a promising solution to meet the structural requirements of mid-rise residential buildings. These sections are commonly fastened using mechanical fasteners such as self-drilling screws, bolts, and Power-Actuated Fasteners (PAF). Nevertheless, the use of these fasteners increases fabrication time, labour requirements, and production costs. Adopting an automated welding method could potentially enable cost-effective mass production of welded CFS built-up sections, thereby reducing manufacturing time and costs. Despite the benefits, applying traditional welding methods like

Metal Inert Gas (MIG), Tungsten Inert Gas (TIG), or Submerged Metal Arc Welding (SMAW) to CFS thin sheets poses challenges due to uncontrolled material deposition, spattering of filler material, excessive heat input, and erosion of the zinc coating. Consequently, there is limited research on appropriate welding processes for CFS sections. Resistance spot welding was investigated by Ungureanu et al. [1] for use on lightweight CFS built-up beams made of corrugated sheet web and built-up steel profiles for the flanges. Moreover, Landolfo et al. [2] evaluated the viability of utilizing laser welding technology in CFS built-up beams. This study attempts to evaluate the applicability of a novel automated welding technology termed Cold Metal Transfer (CMT) on CFS back-to-back welded unlipped channels. A series of welding trials were conducted and calibrated welding parameters are presented. A total of thirty lap shear specimens in all were fabricated utilizing the CMT welding technique to evaluate its ultimate load-carrying capacity and modes of failure.

2 EXPERIMENTAL PROGRAM

2.1 Dimension of lap shear specimen

The dimension of the lap shear specimen for the unlipped channel lap shear specimen is depicted in Fig. 1. The thickness (t) of the unlipped channel was 1.5 mm and the flange (h) of the unlipped channel was kept at 30 mm. The weld length of the lap shear specimen (l_{w_1}, l_{w_2}) was chosen as $15, 20,$ and 25 mm. The length (L) of the single unlipped channel cross-section was kept at 200 mm and the end distance of the flare v-groove weld lap shear specimen was kept at 30 mm based on preliminary test results. The preliminary test results indicated that edge distance (e) and length of the single channel cross-section (L) did not play a role in determining the ultimate shear strength capacity (P_{exp}) of the longitudinal CMT flare v-groove weld, as reported previously by Teh and Hancock [4]. Thus, e and L were kept constant as 30 mm and 200 mm respectively for all the lap shear specimens.

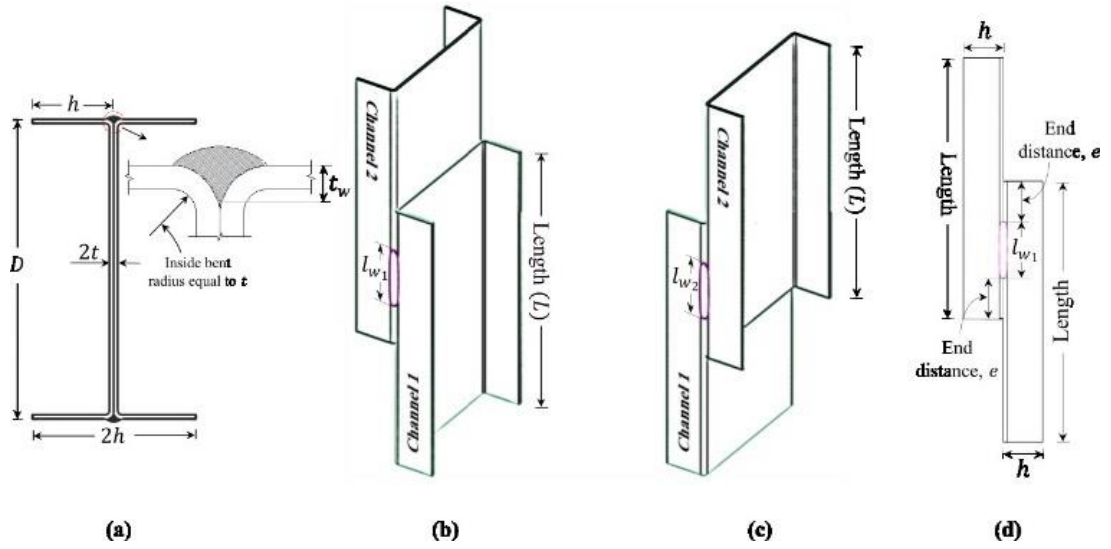

Figure 1 (a) Cross-section of lap shear specimen; (b) View showing the top side of the welding; (c) View showing the bottom side of the welding; (d) Front view of the top side of welding

2.2 Welding parameters for fabrication of lap shear specimen

Fronius TPS 320i CMT welding machine [6] was used for fabricating the lap shear specimens. A semi-automatic welding setup was equipped along with the CMT welding machine to achieve a precise and accurate weld pool of the lap shear specimen without any human intervention. The welding parameters chosen should be such that concluding remarks on the structural performance of CMT Flare v-groove welds can be deduced based on the thickness of weld, t_w. The thickness of weld, t_w is however dependent on the welding current (A), wire feed rate (WFR), and carriage speed (CS) of the welding torch [7]. The welding parameters had to be chosen such that the thickness of weld, t_w remains in the range of $t \leq t_w < 2t$ where $t =$ thickness of the parent sheet metal welded together [8]. Thus, several welding trials were conducted with various combinations of welding current (A) and carriage speed (CS) where the welding current was varied from 110 Amperes to 150 Amperes and the carriage speed of the welding torch (CS) was varied from 220 mm/min to 740 mm/min. A copper-coated steel wire, ER70S-6 conforming to AWS A5.18 [9] of diameter 1.2 mm was used as filler material. The shielding gas used had a mixture of 80% Argon + 20% CO_2 by volume. Metallographic techniques were used in the current study to measure t_w as per Figure J2.6-5 of AISI design standard [8].

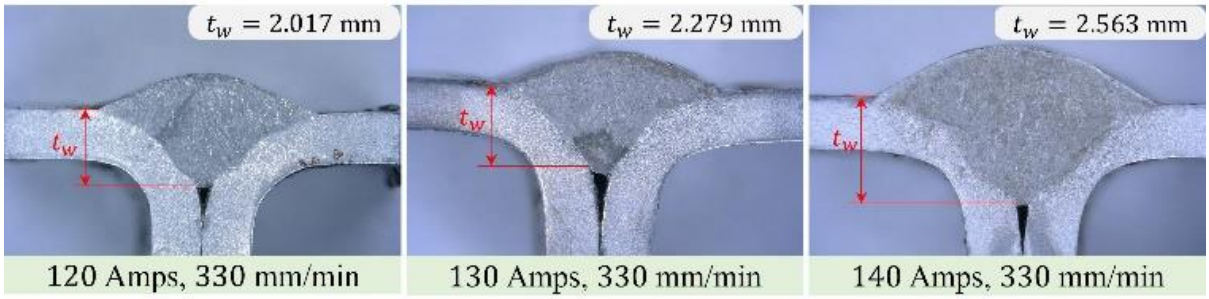

Figure 2 Macroscopic images of calibrated welding parameters

Welding samples were extracted perpendicular to the welding direction by using an abrasive cutting machine. Silicon carbide polishing papers were used to polish the cut surfaces followed by chemical etching using 10% Nital etchant (Nitric acid + Ethanol) [10] to obtain a distinctive diffusion layer of filler material into the parent material. The etched surface was observed under an optical microscope to obtain the weld bead geometry and determine the thickness of the weld, t_w. The observation of the optical macroscopic images (Fig. 2) was calibrated to obtain weld parameters such that satisfactory evenly distributed welding bead in the v-groove (without full penetration of the parent material) can be achieved and thereby also satisfies $t \leq t_w < 2t$ [8] to study the effect of thickness of the weld, t_w on the longitudinal shear strength of CMT flare v-groove welds. The chosen welding parameters are presented in Table 1. A total of 15 lap shear specimens were fabricated as depicted in Table 2.

Table 1 Chosen welding parameters for fabrication of lap shear specimen

Welding Parameter	Current (A) in Amperes	Voltage (V) in Volts	Carriage Speed (CS) in mm/min	t_w/t
W1	120	11.2	330	$\simeq 1.33$
W2	130	11.3	330	$\simeq 1.50$
W3	140	11.4	330	$\simeq 1.67$

Table 2 Test matrix of lap shear specimen

Specimen ID	Cross-section dimension of individual section in mm				Weld length ($\boldsymbol{l_w}$)	
	Thickness (t)*	Flange (h)	Web (D)	End distance (e)	Top (l_{w1}) in mm	Bottom (l_{w2}) in mm
C-W1-25-1	1.5	30	110	30	25.2	27.2
C-W1-25-2	1.5	30	110	30	27.0	25.1
C-W2-25-1	1.5	30	110	30	23.9	24.2
C-W2-25-2	1.5	30	110	30	27.6	26.8
C-W3-25-1	1.5	30	110	30	25.6	24.7
C-W3-25-2	1.5	30	110	30	25.0	27.0
C-W1-20-1	1.5	30	110	30	19.4	21.5
C-W1-20-2	1.5	30	110	30	21.2	21.4
C-W2-20-1	1.5	30	110	30	21.4	23.0
C-W2-20-2	1.5	30	110	30	19.2	18.1
C-W3-20-1	1.5	30	110	30	21.5	21.7
C-W3-20-2	1.5	30	110	30	21.7	21.2
C-W1-15-1	1.5	30	110	30	15.0	14.2
C-W1-15-2	1.5	30	110	30	13.1	14.4
C-W2-15-1	1.5	30	110	30	16.2	17.9
C-W2-15-2	1.5	30	110	30	18.4	16.5
C-W3-15-1	1.5	30	110	30	17.5	17.8
C-W3-15-2	1.5	30	110	30	18.2	17.9

2.3 Lap shear test setup

MTS Landmark 250 kN Fatigue Testing Machine was used to test the lap shear specimen as shown in Fig. 3. The load was applied at a constant rate of 0.5 mm/min using a displacement-controlled loading method. A data acquisition system at a frequency of 10 Hz was equipped to record the load and corresponding displacement of lap shear specimen.

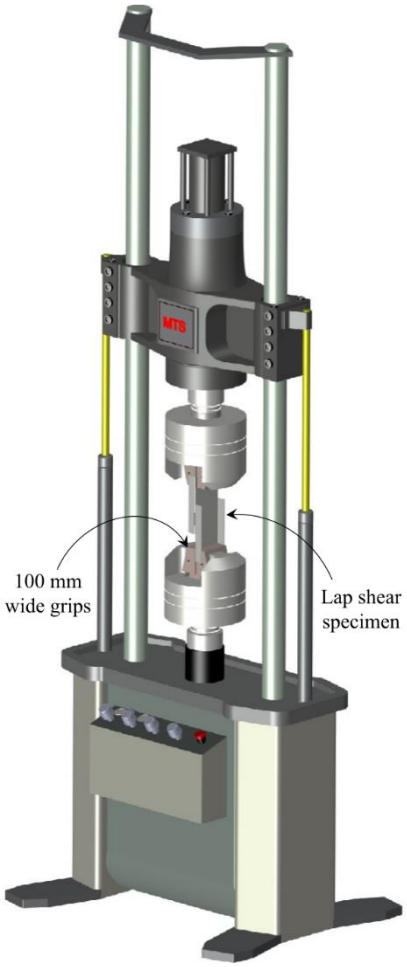

Figure 3 Lap shear test setup

3 RESULTS AND DISCUSSION

The test results including the ultimate longitudinal shear strength (P_{exp}) and the failure modes of the lap shear specimens are summarized in Table 3. In general, all the test specimens failed in either transverse plate tearing of the parent material (in the direction perpendicular to the applied load) [Fig. 4(a-b)] or tangential weld failure at the weld contours (along the direction of the applied load) [Fig. 4(c-d)]. The ultimate load (P_{exp}) versus the axial displacement for all the test specimens along with the corresponding failure modes observed are shown in Figs. 5-9. A detailed description of the observed failure modes and the influencing material and geometric properties are discussed below.

3.1 Plate tearing behavioural feature

A total of 10 out of 18 lap shear specimens failed in transverse plate tearing type failure mode (Table 2). All the test specimens of set 25 mm weld length failed in plate tearing type failure mode. The tearing initiated at the tension ends of the weld (near web-flange interaction) is shown in Fig. 4(a-b). The transverse plate tearing was accompanied by out-of-plane

deformation of individual sections (Fig. 5). The load displacement curve for the specimen set of weld length 25 mm is shown in Fig. 6. The lap shear specimen of set 20 mm weld length too experienced plate tearing failure mode except C-W1-20-1 and C-W2-20-2 (Fig. 7).

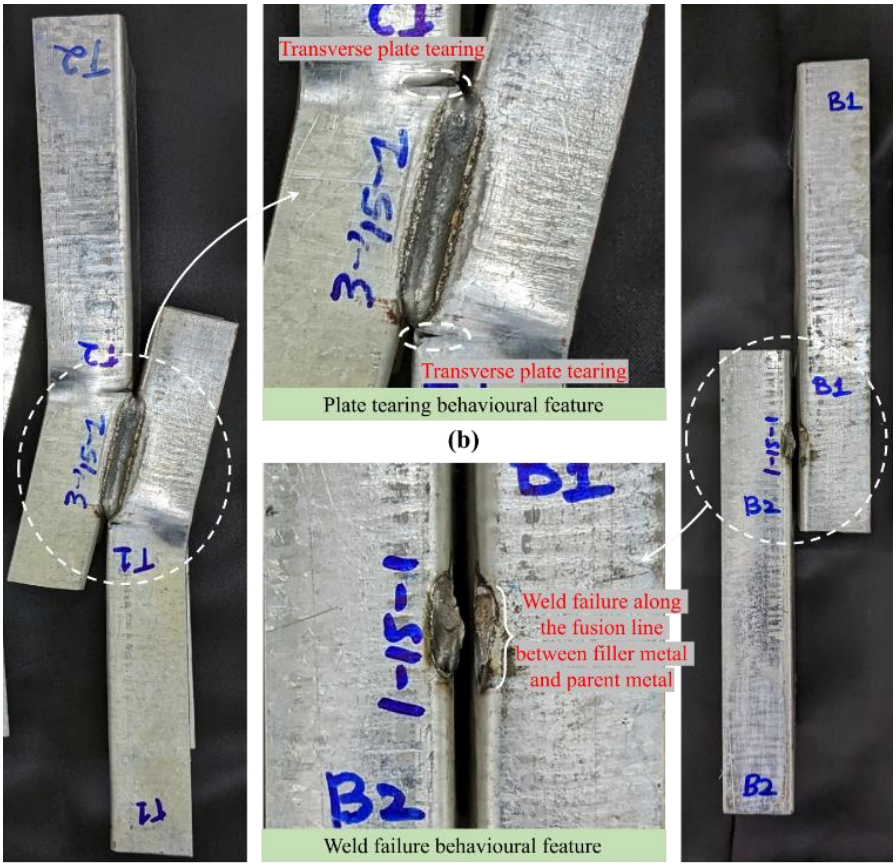

Figure 4 (a-b) Plate tearing behavioural feature; (c-d) Weld failure behavioural feature

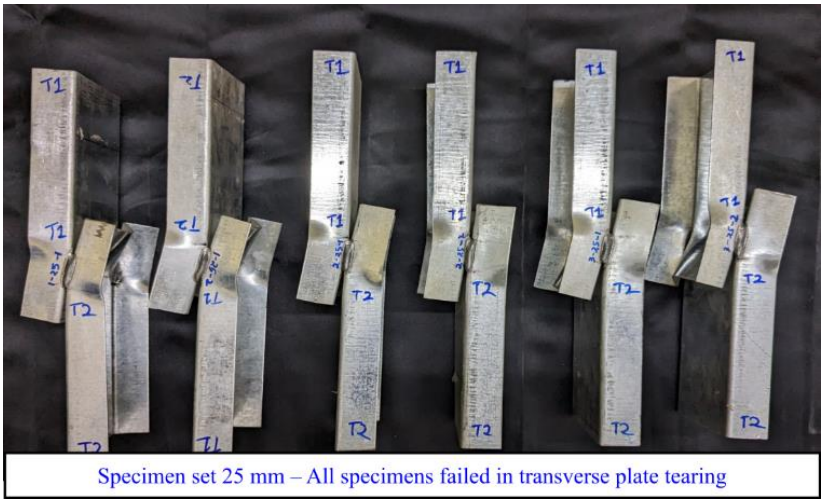

Figure 5 Failure modes of specimen set 25 mm

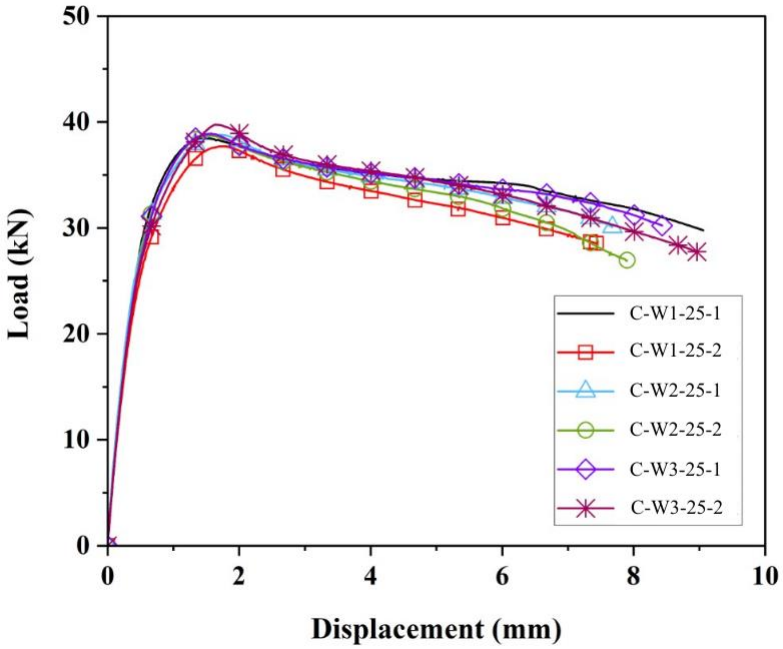

Figure 6 Load-displacement of specimen set 25 mm

Figure 7 Failure modes of specimen set 20 mm

3.2 Weld failure behavioural feature

A total of 8 out of 18 lap shear specimens experienced weld failure (refer to Table 2). The specimens of set 15 mm weld length (Fig. 8) and C-W1-20-1 and C-W2-20-2 of specimen set 20 mm weld length (Fig. 7) failed in weld failure along the weld contours [Table 2]. None of

the failures was completely through the weld pool of the lap shear specimens. The failure initiated at the tension end of the weld (near the web-flange intersection) and further propagated along the weld contours (taking the path of least resistance) where shearing off the fusion line [Fig. 4(c-d)] between the filler material and parent material was observed. The weld failure was observed after reaching the ultimate shear strength, as can be observed from the load-displacement plots of specimen set of 20 mm weld length and 15 mm weld length [Fig. 9, 10].

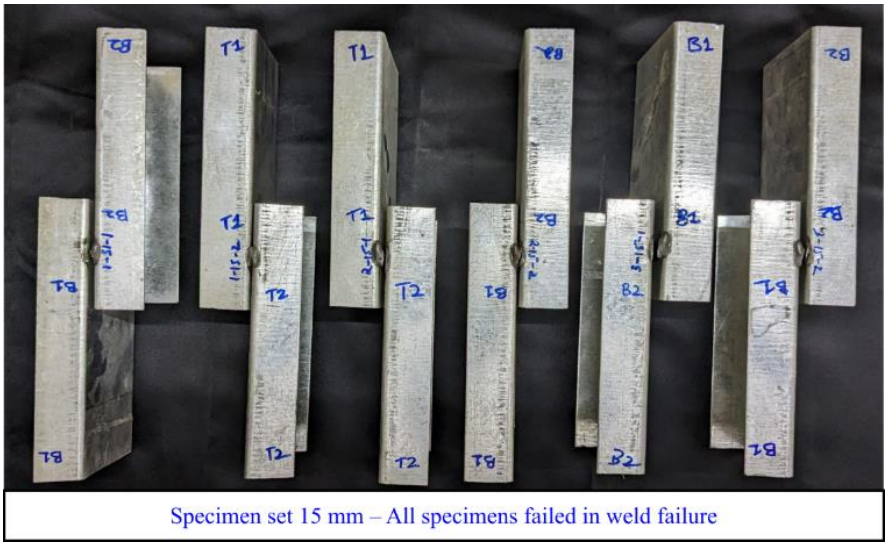

Figure 8 Failure modes of specimen set 20 mm

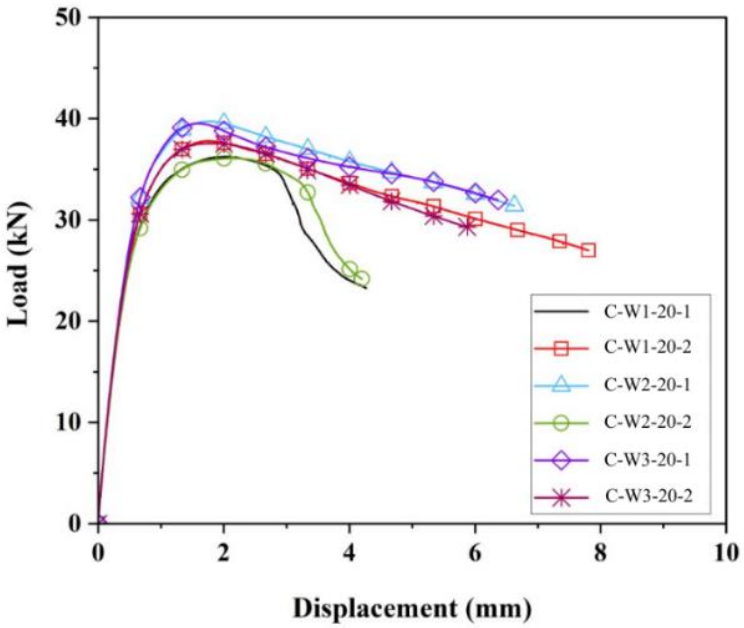

Figure 9 Load-displacement of specimen set 20 mm

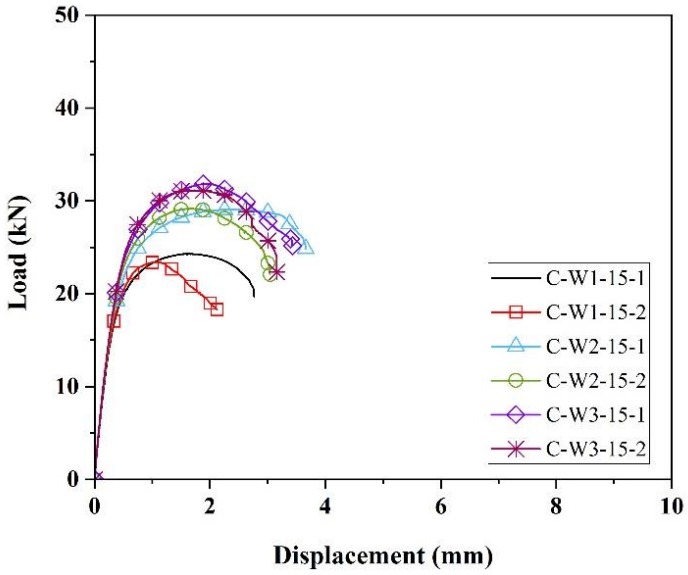

Figure 10 Load-displacement of specimen set 15 mm

3.3 Factors influencing the failure mode of flare v-groove welds

Table 2 shows the failure modes observed for the flare v-groove welds subjected to longitudinal loading. As mentioned in Section 3.2, the lap shear specimens in the set 20 mm weld length failed in both plate tearing type failure and weld failure along the weld contours (Table 2). However, the lap shear specimen of weld length 25 mm failed in plate tearing failure type whereas specimens of set 15 mm failed in weld failure. This observation thus substantiates that weld length (l_w) is one of the deciding parameters in determining the failure mode. Additionally, the outstanding flange length (h), the ultimate tensile strength of the electrode (f_{xx}), and the ultimate tensile strength of the parent material (f_u) will be responsible for transfer of tensile forces and shear forces at the junction of the weld pool and individual cross-section. Thus, the parameters which decide the failure mode includes:

a) Length of the weld (l_w)
b) Outstanding flange length (h)
c) Ultimate tensile strength of electrode (f_{xx})
d) Ultimate tensile strength of parent material (f_u)

Thus, a limiting ratio ($L.R.$) based on the above observation is proposed which can determine the failure mode of CMT Flare-v groove welds subjected to longitudinal loading.

$$L.R. = \frac{l_w f_{xx}}{h f_u} \qquad (1)$$

For the specimens experiencing plate tearing behavioural feature, $L.R. \geq 1$. Whereas, for specimens experiencing weld failure behavioural feature, $L.R. < 1$. Table 3 illustrates that the

proposed limiting ratio agrees with the experimental test results. Figure 11 represents the limiting ratio.

3.4 Lacunae in AISI Design standard

Section J2.6 of AISI S100 [8] provides design equation for predicting the ultimate longitudinal shear strength capacity of flare v-groove welds (P_{AISI}). According to AISI design standard,

For $t \leq t_w < 2t$ or if the lip height, h is less than weld length, L :

$$P_{AISI} = 0.75tLf_u \quad (2)$$

where, P_{nv} = Nominal longitudinal shear strength of flare groove weld [8]. In the current study, it was made sure using metallographic techniques that the thickness of weld, t_w does not exceed $2t$. Hence, Eq. 2 is applicable for the current scenario. However, in the present investigation, the unlipped channel was welded back-to-back via CMT flare v-groove weld on either side of the flange-web intersection. Hence, the total weld length, L as per AISI [8] should be calculated as,

$$L = 2 \times l_w \text{ where } l_w = \text{Minimum of } (l_{w1}, l_{w2})$$

Thus, $$P_{AISI} = 2 \times (0.75tl_wf_u) \quad (3)$$

Table 3 shows the comparison of experimental test results with AISI design standard [8]. Equation 3 depicts the linear relationship of ultimate longitudinal strength (P_{AISI}) with the length of the weld (l_w). However, the current experimental results do not vary linearly with the length of the weld (Table 3). Moreover, Table 3 illustrates the over-conservativeness of the AISI design provisions [8] by 143% (Fig. 11). Thus, it is suggested to revise the design guidelines for determining ultimate shear strength of flare v-groove welds subjected to longitudinal loading.

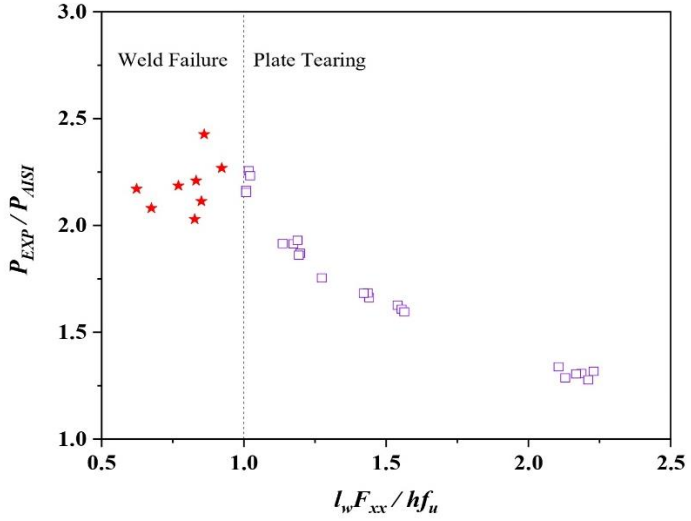

Figure 11 Limiting ratio and over-conservative AISI predictions

Table 3 Experimental results and comparison with AISI design standard

Specimen ID	P_{exp} in kN	l_w in mm	$\frac{l_w f_{xx}}{h f_u}$	Failure mode+	P_{AISI} in kN	$\frac{P_{exp}}{P_{AISI}}$
C-W1-25-1	38.46	25.20	1.20	PT	20.57	1.87
C-W1-25-2	37.69	25.10	1.19	PT	20.26	1.86
C-W2-25-1	38.79	23.90	1.14	PT	20.31	1.91
C-W2-25-2	38.71	26.80	1.27	PT	22.12	1.75
C-W3-25-1	38.92	24.70	1.17	PT	20.38	1.91
C-W3-25-2	39.74	25.00	1.19	PT	20.59	1.93
C-W1-20-1	36.24	19.40	0.92	WF	15.96	2.27
C-W1-20-2	37.79	21.20	1.01	PT	17.50	2.16
C-W2-20-1	39.75	21.40	1.02	PT	17.59	2.26
C-W2-20-2	36.16	18.10	0.86	WF	14.88	2.43
C-W3-20-1	39.52	21.50	1.02	PT	17.72	2.23
C-W3-20-2	37.61	21.20	1.01	PT	17.49	2.15
C-W1-15-1	24.33	14.20	0.68	WF	11.70	2.08
C-W1-15-2	23.42	13.10	0.62	WF	10.79	2.17
C-W2-15-1	29.07	17.40	0.83	WF	14.32	2.03
C-W2-15-2	29.16	16.20	0.77	WF	13.32	2.19
C-W3-15-1	31.84	17.50	0.83	WF	14.41	2.21
C-W3-15-2	31.15	17.90	0.85	WF	14.76	2.11

+ PT – Plate tearing; WF- Weld failure h = 30 mm for all lap shear specimens as per AISI [8]

l_w = Minimum of l_{w1} and l_{w2} f_u = 366 MPa as per coupon test results

f_{xx} = 522 MPa as per research carried out by Ermakova et al. [11]

4 CONCLUSION

The structural performance and quality of a novel welding technique called Cold Metal Transfer welding technology are assessed using metallographic techniques and the feasibility of its application in CFS sections is verified using a component-based study. Lap shear tests were carried out to assess the structural performance of CMT flare v-groove welds on back-to-back connected CFS sections subjected to longitudinal shear. The lap shear specimens failed in either of the two modes i.e., transverse plate tearing of the individual cross-section and weld failure near the weld contours. The parameters that influenced the failure mode of the lap shear specimen are weld length (l_w), outstanding flange length (h), ultimate tensile strength of the parent material (f_u), and ultimate tensile strength of the filler wire electrode (f_{xx}). The experimental results showed that AISI is over-conservative by a maximum of 143% and is unable to predict the failure mode of the longitudinal flare v-groove welds accurately. Thus, a limiting ratio constituting these influencing parameters is presented to determine the failure mode.

REFERENCES

[1] Ungureanu, V., Both, I., Burca, M., Radu, B., Neagu, C., and Dubina, D. (2021). "Experimental and numerical investigations on built-up cold-formed steel beams using resistance spot welding." Thin-Walled Structures, 161, 107456.

[2] Landolfo, R., Mammana, O., Portioli, F., Di Lorenzo, G., and Guerrieri, M. (2009). Experimental investigation on laser welded connections for built-up cold-formed steel beams." Journal of Constructional Steel Research, 65(1), 196–208

[3] Teh, L. H. and Hancock, G. J. (2002a). "Strength and behavior of fillet welded connections in g450 sheet steel.

[4] Teh, L. H. and Hancock, G. J. (2002b). "Strength and behavior of flare-bevel and flare-vee welded connections in g450 sheet steel.

[5] Teh, L. H. and Hancock, G. J. (2005). "Strength of welded connections in g450 sheet steel." Journal of Structural Engineering, 131(10), 1561–1569

[6] Fronius. "https://www.fronius.com/en." Fronius, Austria.

[7] Karadeniz, E., Ozsarac, U., and Yildiz, C. (2007). "The effect of process parameters on penetration in gas metal arc welding processes." Materials Design, 28(2), 649–656.

[8] AISI (2016). "North american specification for the design of cold-formed steel structural members." AISI S100-16, AISI

[9] AWS (2018). "Specification for carbon steel electrodes and rods for gas shielded arc welding." AWS A5.18/A5.18M, AWS.

[10] Magda, A., Popescu, M., Codrean, C., and Mocuta, E. (2013). "Possibilities of joining galvanized sheet steel using the cmt method (cold metal transfer)." Welding International, 27(9), 665–667.

[11] Ermakova, A., Mehmanparast, A., Ganguly, S., Razavi, J., and Berto, F. (2020). "Investigation of mechanical and fracture properties of wire and arc additively manufactured low carbon steel components." Theoretical and Applied Fracture Mechan-ics, 109, 102685